Synthesis and Characterization of Bi_2O_3: Sb Nanostructured Thin Films
Prepared by Chemical Spray Pyrolysis Method

Mohammed I. Karim* Ziad T. Khodair Asaad A. Kamil
Department of Physics, College of Sciences, University of Diyala
Sciphms222310@uodiyala.edu.iq Ziad_tariq70@yahoo.com Asaad181162@yahoo.com

Abstract :
In the present work, thin films of undoped bismuth oxide (Bi2O3) and bismuth oxide doped with antimony (Bi2O3: Sb) were deposited on glass substrates by using the chemical spray pyrolysis process. We prepared the films with various weight percentages of antimony (0, 3, 5, 7, and 9 wt%). Throughout the experiment, the substrate was maintained at a consistent temperature of 380°C for the deposition operation. The goal of this study is to investigate the effects of antimony doping on the structural and optical characteristics of the Bi2O3 film. We studied the structural and optical properties of the prepared thin films using x-ray diffraction (XRD), atomic force microscopy (AFM), and ultraviolet-visible spectroscopy (UV-VIS). The X-ray diffraction results showed that the prepared films were polycrystalline with a tetragonal structure. Thin films of Sb doped Bi2O3 demonstrated increasing absorption with increasing the concentration of the dopant . The measured energy gap value for undoped Bi2O3 was 3.04 eV. Increasing the concentration of the antimony dopant led to a decrease in the energy gap value (from 3.04 to 2.48 eV). Undoped bismuth oxide and 9% Sb doped bismuth oxide were deposited on porous silicon, as it is used in solar cell manufacturing. The solar cell features were evaluated.

Keywords: Bismuth oxide, Thin films, Optical properties, Optoelectronic applications.

تحضير وتوصيف أغشية Bi_2O_3: Sb الرقيقة نانوية التركيب باستعمال طريقة التحلل الحراري الكيميائي بالرش

محمد اسماعيل كريم زياد طارق خضير اسعد احمد كامل
جامعة ديالى – كلية العلوم – قسم الفيزياء

الخلاصة:
في العمل الحالي ، تم ترسيب أغشية رقيقة من أوكسيد البزموث غير المطعم (Bi_2O_3) وأوكسيد البزموث المطعم بالانتيمون (Bi_2O_3: Sb) على قواعد زجاجية بطريقة التحلل الحراري الكيميائي بالرش. حضرت الأغشية بنسب وزنية مختلفة للانتيمون (0،3،5،7و9%) تم تثبيت درجة حرارة القاعدة عند 380 درجة مئوية خلال التجربة طيلة عملية الترسيب. الهدف من هذه الدراسة هو التحقق من تأثير التطعيم بالانتيمون على الخصائص التركيبية والبصرية لأوكسيد البزموث .قمنا بدراسة الخواص التركيبة والبصرية لأغشية الرقيقة المحضرة باستخدام حيود الأشعة السينية (XRD) ، مجهر القوة الذرية (AFM) والطيف المرئي فوق البنفسجي ((UV–VIS). بينت نتائج حيود الأشعة السينية أن الأغشية المحضرة هي متعددة التبلور ومن النوع الرباعي .أظهرت أغشية أوكسيد البزموث المطعم بالانتيمون زيادة بالامتصاصية مع زيادة تركيز الشائبة. قيست قيمة فجوة الطاقة لأغشية أوكسيد البزموث غير المطعم وكانت (3.04 ألكترون فولت) ، ان زيادة تركيز شائبة الأنتيمون يؤدي الى نقصان قيمة فجوة الطاقة. تم ترسيب أوكسيد البزموث غير المطعم وأوكسيد البزموث المطعم بنسبة 9% أنتيمون على السيلكون المسامي، اذ استعمل لتصنيع الخلية الشمسية وتم حساب خصائص الخلية الشمسية.

الكلمات المفتاحية : اوكسيد البزموث، اغشية رقيقة، الخصائص البصرية، التطبيقات الضوئية.

* Corresponding author : Mohammed I. Karim

1- Introduction

The scientific community has become interested in heavy metal oxides, especially Bi_2O_3, because they have important uses in optical and electrical equipment, glass ceramics, thermal and mechanical sensors, and layers that let infrared light through [1-3].

Thin-film bismuth oxide (Bi_2O_3) exhibits photoluminescence, a strong band gap, and the Hall Effect, making it a material of interest. [4–6]. Researchers have reported five different forms of bismuth oxide, known as a-, b-, c-, d-, and x- Bi_2O_3. Two of them, the low-temperature and the high-temperature phases, are stable; however, the others are high-temperature meta-stable phases [7-8]. The phase relations in the case of the Bi-O system and the chemical bonding of Bi_2O_3 polymorphs, which play an important role in the oxidation processes of Bi, Recent publications have addressed [9-11] because of the theoretical and experimental significance, the optical properties of bismuth oxides were studied [12–16]. Nanomaterials are becoming increasingly popular due to their unique optical, magnetic, electrical, and other capabilities [17]. Emerging properties offer significant potential for applications in electronics, medicine, and other sectors. Commercial products and processes widely employ engineered nanoparticles, while some naturally occur. They also have medical applications for diagnosis, imaging, and drug delivery [18].

Researchers have developed various physical and chemical approaches to improve the characteristics of nanomaterials, allowing for better control over particle size and distribution during synthesis. Nanomaterials can be synthesized using either top-down or bottom-up approaches. The former involves dissociating bulk solids into finer particles, while the latter involves assembling atoms together [19-20].

Various methods can be used to deposit Sb-doped Bi_2O_3 thin films, such as vacuum evaporation, chemical vapour transport, pulsed laser deposition, electrodeposition, sputtering , chemical bath deposition technique, and spray pyrolysis. Among these methods, spray pyrolysis was chosen in this paper due to many advantages, such as being very simple, cost-effective , and multilayered [21-23].

This paper deals with the electrical and optical analysis of chemical spray pyrolysis Sb doped Bi_2O_3 thin films.

2-Experimental procedure

Borosilicate glass substrates with dimensions of 2.5×2.5 cm2 and a thickness of 0.1 cm were prepared by cutting large microscope slides. The prepared glass substrates were first carefully cleaned by boiling them in chromic acid for 15 minutes, Then, they were rinsed with double-distilled water. We then immersed the glass substrates in acetone to remove organic impurities. The substrates underwent an additional 15 minutes of ultrasonic treatment before depositing.

The solution of bismuth nitrate (0.2 M) in 100 ml was prepared by dissolving 9.7014 g of the bismuth nitrate pentahydrate ($Bi(NO_3)_3.5H_2O$ salt in 100ml of dilute nitric acid. The solution of antimony(III) chloride (0.2M) was prepared by dissolving (4.5626 gm) of $SbCl_3$ in 100 ml of glacial acetic acid. We prepared the mixture by combining bismuth nitrate and antinomy(III) chloride in various ratios, resulting in different concentrations of Sb (0, 3, 5, 7, 9) wt%.

Then the glass substrates were heated up to 380 ± 5ºC. We placed the nozzle tip about 30 cm above the substrate surface. The air pressure was adjusted to 1.5 bar to transform the droplets into a spray. We filled the bulb of the nozzle with 100 ml of a specific precursor solution for each thin film preparation experiment.

We obtained the X-ray diffraction patterns for the prepared films using a Shimadzu XRD-6000 goniometer and recorded atomic force microscopy (AFM) micrographs using a scanning probe microscope type (SPM-AA3000), contact mode, supplied by Angstrom Advanced Inc. We investigated optical properties in the wavelength range of 300-900 nm using UV-VIS-NIR spectroscopy (Shimadzu, UV-1800).

3-Results and discussions

3-1 XRD analysis:

Figure (1) displays the X-ray diffraction (XRD) patterns of Sb-doped Bi_2O_3 thin films. Diffraction peaks may be seen in the pattern at ($2\theta \sim 27^o, 31^o, 34^o, 46^o, 54^o$). The tetragonal and polycrystalline structure of the produced Bi_2O_3 thin films aligns with other publications [24]. All of the peak positions correspond to the (221), (002), (400), (402), and (223) planes, respectively; these outcomes match the (ICDD) card number. Matching results (01-074-1374): Figure 1 The strongest peak appears at 2θ~27° in the (221) plane.

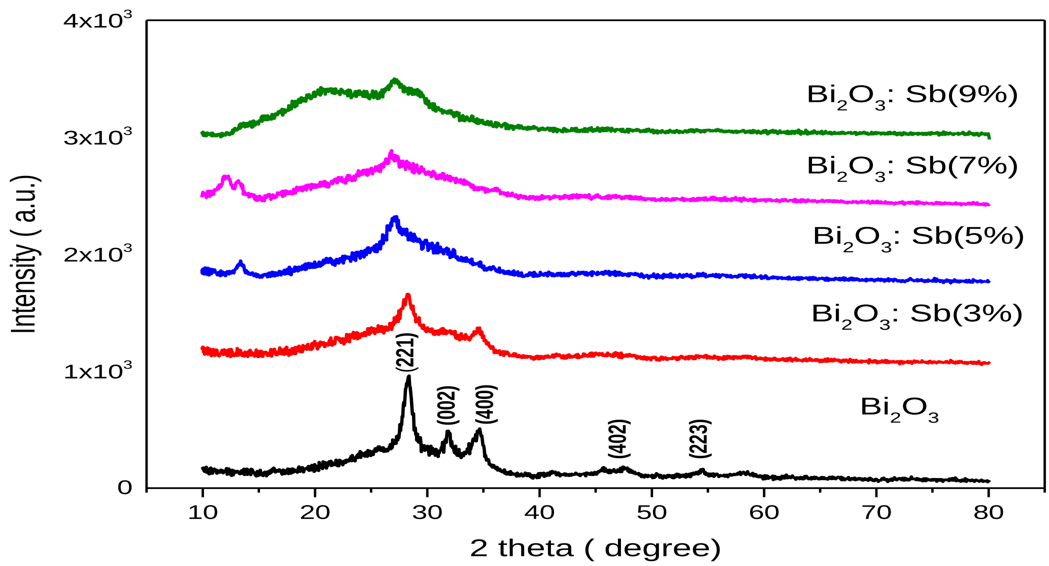

Figure (1) : The XRD pattern for undoped and Sb-doped Bi_2O_3 thin films.

3-1-1 Crystallite Size (D):

We used the Scherer method to calculate the average grain size (Dav) for the dominant (002) direction, using the following formula [23,24]:

$D_{av} = K\lambda / \beta \cos\theta$.......(1)

Where D_{av} is the crystallite size, K is a constant known as the shape factor (0.94), λ is x-ray wavelength = 0.1506 nm, β is the full width at half maximum (FWHM), given in radians, and θ is the Bragg's angle. We observe a decrease in the average grain size as the doping ratio increases, with the exception of the 3% and 7% Sb ratios. Table 1 shows the value of the average grain size for Sb-doped Bi_2O_3 thin films.

Table (1) : value of the average grain size for undoped and Sb-doped Bi_2O_3 thin films

Samples	**D_{av} (nm)**
Undoped- Bi_2O_3	7.521
Bi_2O_3:Sb (3%)	9.284
Bi_2O_3:Sb (5%)	8.792
Bi_2O_3:Sb (7%)	11.401
Bi_2O_3:Sb (9%)	9.746

3-1-2 Dislocation Density and Number of Grains

The quantity of defects in a crystal is measured by its dislocation density (δ), which was calculated using the following equation [25]:

$\delta = 1/D_{av}^2$ ....(2)

The number of crystallites (N_o), which stands for the number of crystals per unit area, was calculated using the following relationships

$N_0 = t / D_{av}^3$...............(3)

Where t is thickness of thin films .

For all thin films, it was discovered that the values of No increase as grain size decreases as shown in table (2) .

Table (2): Structural parameters of undoped and Sb-doped Bi_2O_3 thin films.

Sample	2θ	FWHM	D_{hkl}	$\varepsilon\times10^{-3}$	$\delta\times 10^{-3}$	N_0
Undoped– Bi_2O_3	28.031	0.897	9.530	3.797	11.010	0.404
	31.723	0.897	9.612	3.764	10.822	0.394
	46.127	2.243	4.019	9.004	61.909	5.391
	54.236	1.346	6.923	5.227	20.863	1.054
Bi_2O_3:Sb(3%)	28.263	0.984	8.692	4.163	13.235	0.510
	32.089	1.18	7.313	4.948	18.694	0.856
	54.363	0.787	11.84	3.054	7.124	0.201
Bi_2O_3:Sb(5%)	27.001	0.787	10.84	3.339	8.512	0.255
	31.705	0.787	10.95	3.303	8.331	0.247
	46.319	1.968	4.583	7.895	47.591	3.374
Bi_2O_3: Sb(7%)	26.910	0.787	10.83	3.339	8.515	0.255
	6.749	0.787	11.48	3.152	7.586	0.214
	55.117	0.787	11.88	3.044	7.076	0.193
Bi_2O_3:Sb(9%)	27.114	0.984	8.670	4.173	13.301	0.490
	32.377	0.787	10.97	3.297	8.303	0.242
	46.397	0.787	11.46	3.156	7.606	0.212
	53.671	.18	7.877	4.594	16.115	0.654

3-2 Atomic Force Microscopy (AFM):

In this investigation, materials with dimensions of ($2x2\mu m^2$) were scanned, and pictures from atomic force microscopy (AFM) were used for observation. Moreover, using RMS values, which are an important indicator of the smoothness or roughness of a surface, we found that as the antimony doping ratio rises, the pure surface's root mean square (RMS) roughness increases as Table 3 illustrates.

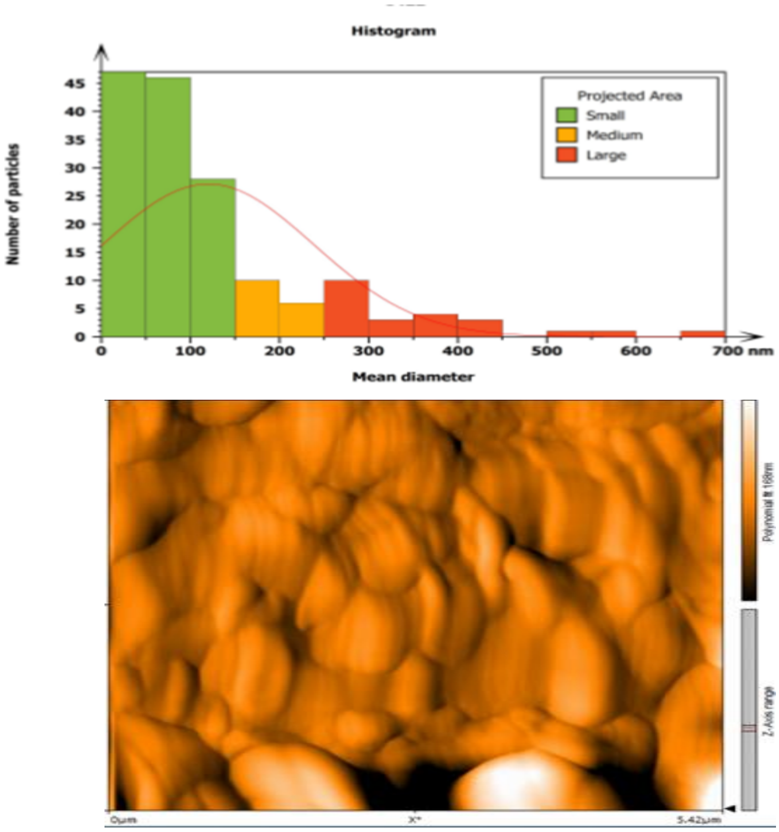
Histogram
Projected Area
Small
Medium
Large
Number of particles
0
5
10
15
20
25
30
35
40
45
0
100
200
300
400
500
600
700 nm
Mean diameter

(a)

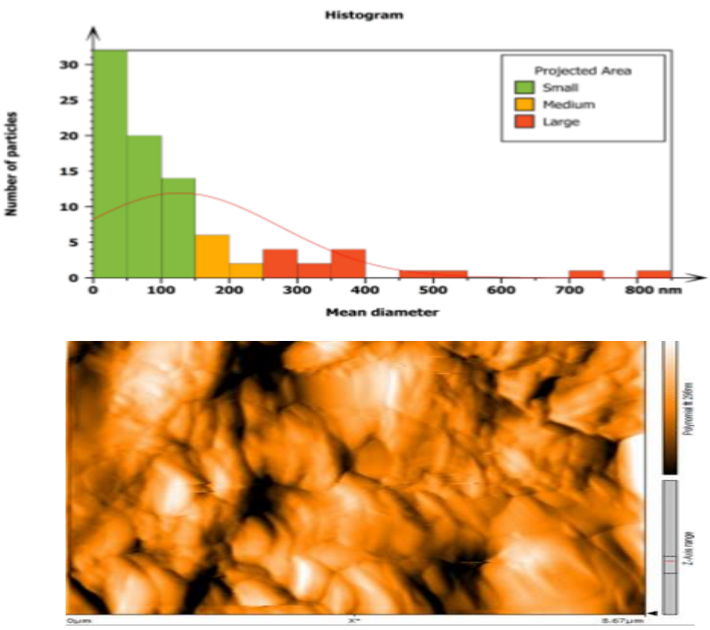
Histogram
Projected Area
Small
Medium
Large
Number of particles
0
5
10
15
20
25
30
0
100
200
300
400
500
600
700
800 nm
Mean diameter

(b)

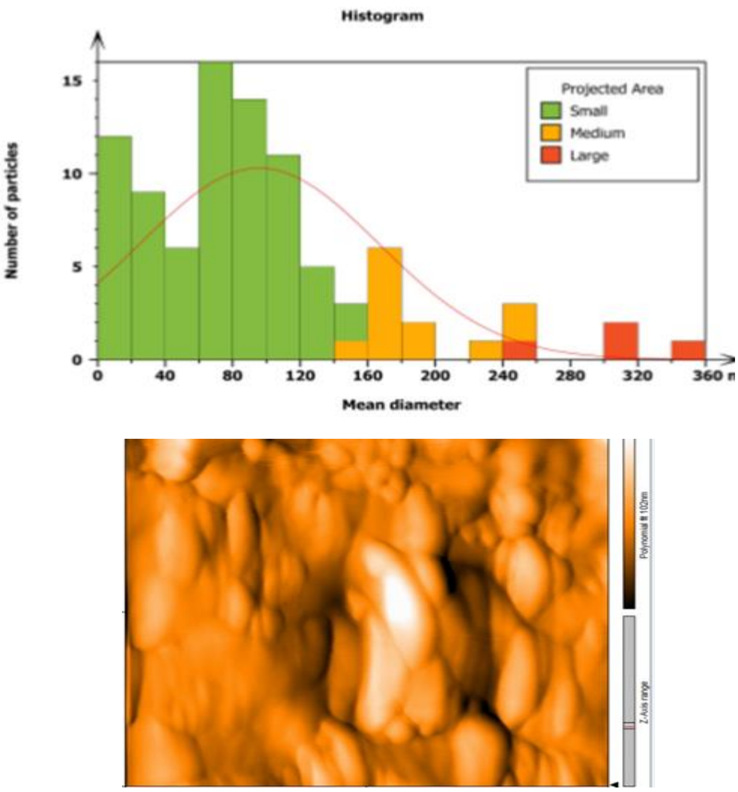

(C)

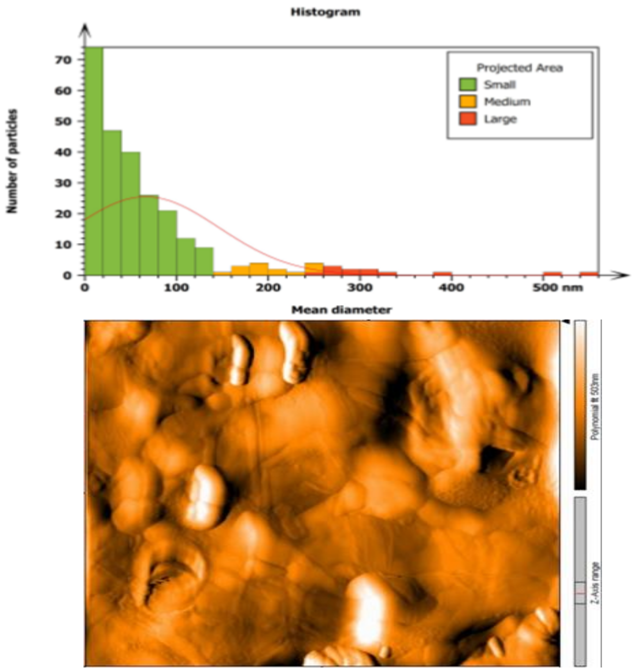

(d)

Figure(2) : 3-Dimensional AFM images of (a) Undoped Bi_2O_3, (b) Bi_2O_3 :5%Sb, (c) Bi_2O_3 :7%Sb, (d) Bi_2O_3 :9%Sb.

Table (3) : The Average root mean square and roughness average for undoped and Sb-doped Bi_2O_3 films.

Sample	Average Roughness Sa	Root Mean Square RMS (nm)	Mean Particle Size (nm)
Undoped-Bi_2O_3	94.27	118	120
Bi_2O_3:Sb 3%	72.08	86.88	53.73
Bi_2O_3:Sb 5%	-	-	126.9
Bi_2O_3:Sb 7%	279.6	336.5	95.75
Bi_2O_3:Sb 9%	195.7	233.7	66.43

3-3 Optical properties:

3-3-1 Transmittance (T):

The relationship between transmittance and wavelength in the (350–900 nm) range is seen in Figure (3) for (0–9)% Sb doped Bi_2O3 thin films; it shows the transmittance curve as a function of wavelength. The transmittance curves showed their increase by increasing the wavelength. It has the lowest transmittance value at a short wavelength, but in the visible spectrum region within the range (400–700 nm), the transmittance begins to increase gradually with increasing wavelength. The transmission's behavior changes as the concentration of Sb doping increases. As the concentration of Sb doping increases, the transmittance of Bi_2O_3 films decreases steadily. Antimony doping creates crystal defects, which may lead to an increase in photon scattering at higher doping concentrations, explaining the decrease in transmittance. Meanwhile, an increase in grain boundary scattering and free carrier absorption accounts for the 33% transmittance increase [22].

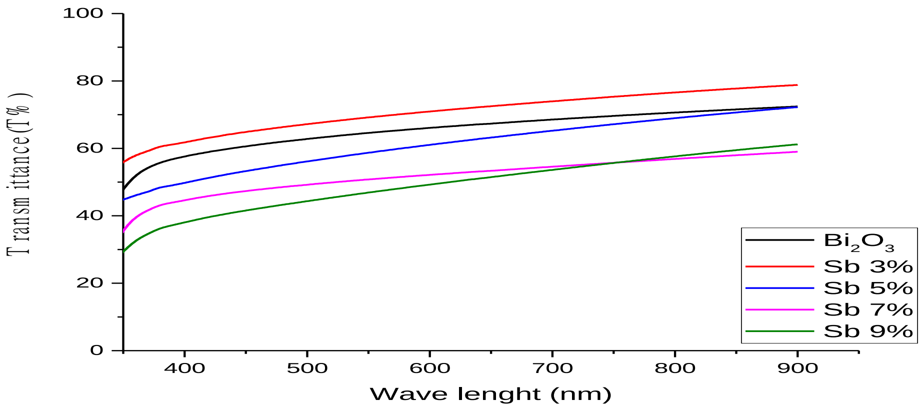

Figure (3): The transmittance spectra of Sb doped and undoped thin films as a function of wavelength.

3-3-2 Optical Energy Gap (E_g)

The optical energy gap (Eg) was calculated by plotting a graph between $(\alpha\ h\upsilon)^2$ and (hυ) in eV, where the extension of the straight part of the curve and its point of unit section with x- axis give the optical energy gap (Eg).

The optical energy gap for Sb-doped bismuth oxide thin films was calculated using the following equation:

$$\alpha h\nu = A(h\upsilon - E_g)^r \quad \ldots\ldots\ldots(4)$$

where A is the constant value that is dictated by the kind of transition, r=1/2 for allowed direct transitions. The energy gap value for undoped - bismuth oxide thin films is equal to (3.04 eV). The energy gap for Sb doped oxide bismuth thin films changes with increasing the doping ratios of Sb concentrations, as shown in Figure 4. Where we notice a decrease in the value of the energy gap, their value is within the range of 2.48- 3.04 eV. This is important for applications using optoelectronic devices. An increase in carrier concentration may trigger the band shrinking effect, leading to a reduction in the optical band. The addition of more antimony atoms to the substitutional sites increased the band gap and the number of occupied states.

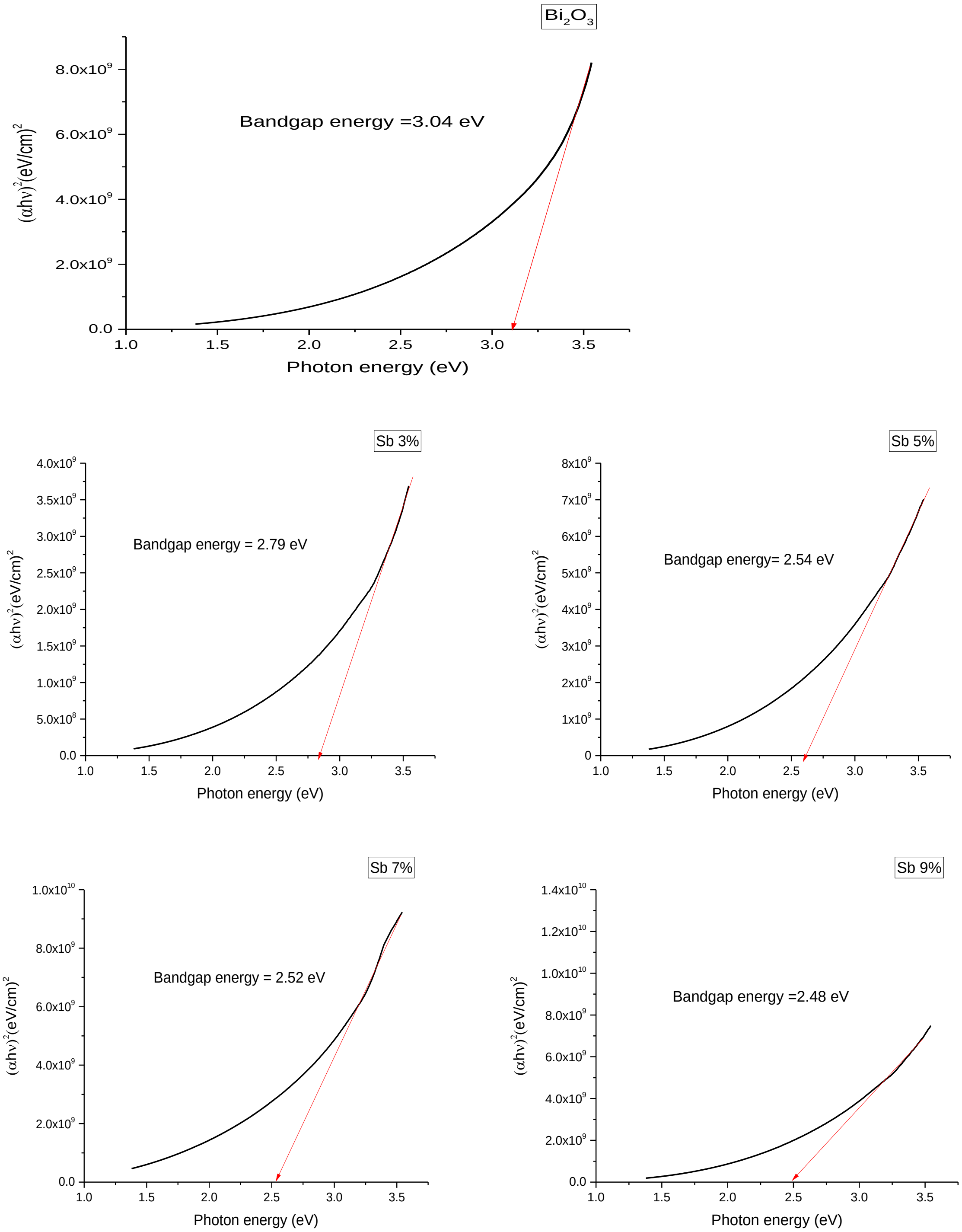

Figure (4): Optical band gap (E_g) of Sb doped and undoped Bi_2O_3 thin films

3-4- Solar cell measurements:

3-4-1 (I-V) Characteristic at dark:

Figure (5) illustrates the current-voltage (I-V) characteristics of the heterojunction for un-doped Bi2O3 and Sb-doped Bi2O3 forward bias and reverse bias at a voltage applied from 1–5 volts. In the forward bias instance, the heterojunction's current develops with increased practical voltage due to its low resistance, but in the reverse bias scenario, no current flows through it due to its high resistance. One consistent characteristic of heterogeneous is the overall behavior of the current, with voltages in the forward and reverse biases [26, 27]. Based on these values, when the heterojunction is under a forward bias, its current increases proportionally to an increase in practical voltage. The current identifies the first of two regions in the recombination process. The forward current of solar cells has relatively low voltages. This current, known as recombination current, occurs only at low voltages. An electron creates a hole when it moves from the conduction band into the valence band. The diffusion or bending region, which is the second region at high voltage, is formed by the series resistance. The current accelerates and grows with the applied voltage in this location—a phenomenon known as drift current—when the bias voltage is high enough to provide electrons with enough energy to cross the barrier separating the two sides of the junction in this region. Drift current is the term for the phenomenon where the current develops and accelerates as the applied voltage increases [28, 29].

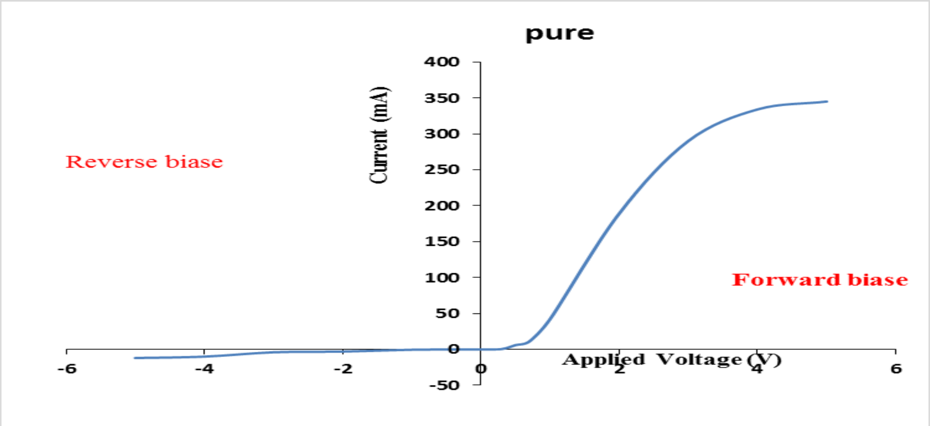

(a)

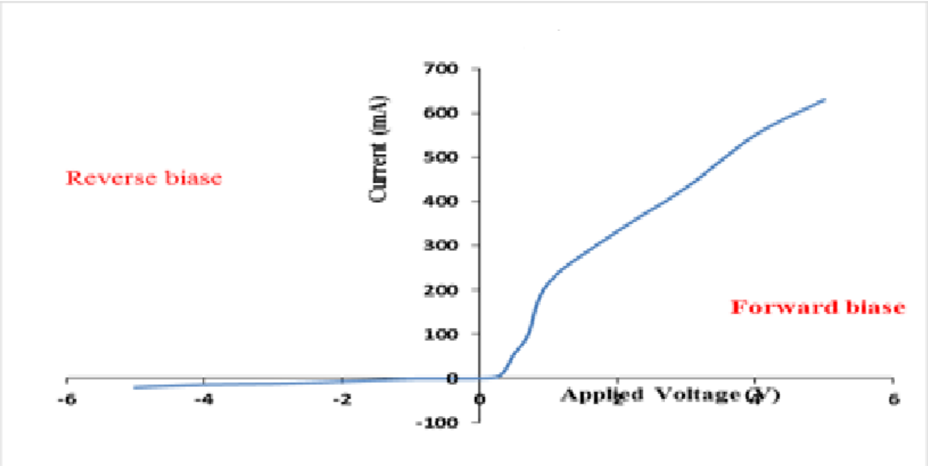

(b)

Figure (5) : I-V Characteristic in the dark for both reverse and forward bias of (a) undoped Bi_2O_3 and(b) 9% Sb doped Bi_2O_3.

3-4-2:(I-V) Characteristic at illumination:

Figures (6) show (I-V) properties in both light and dark, producing photocurrent when illuminated by a (100 mWm^{-2}) tungsten lamp. Remember, p-Si uses the cell's effective area of 0.78 cm^2. Increasing the applied voltage and incident light intensity causes the optical current to increase. This, in turn, widens the depletion region and increases the number of charge carriers, which in turn promotes electron absorption and production. It is noticed that the illuminated current value is larger than that of the current value in the dark case. In this case, photons impact the heterojunction, causing a greater movement of charge carriers (electrons), leading to an increase in current, independent of voltage.

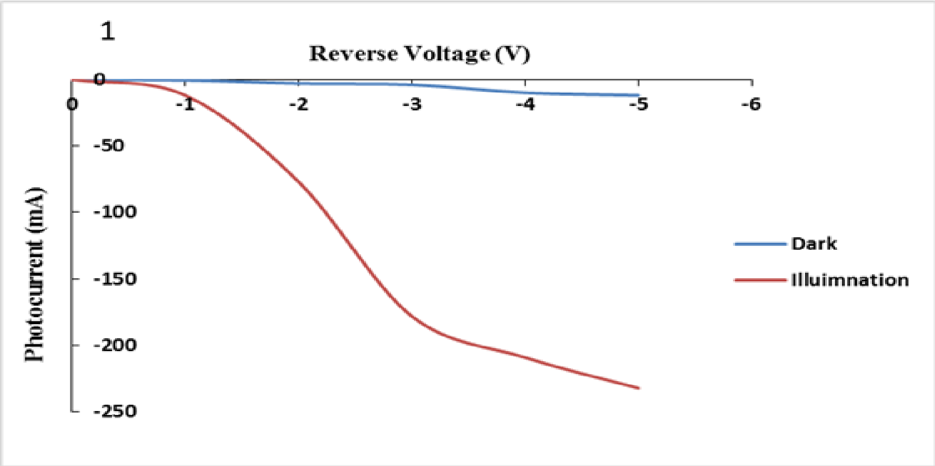

(a)

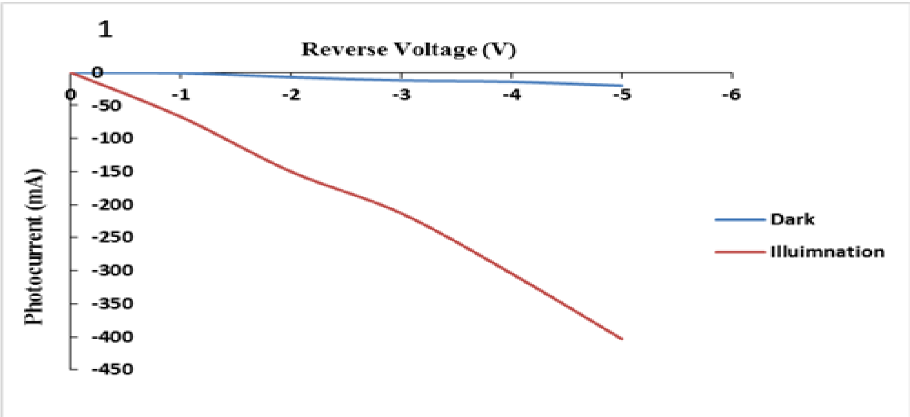

(b)

Figure (6): I-V Characteristic in the illumination for both reverse and forward bias of (a) undoped Bi_2O_3 and (b) 9% Sb doped Bi_2O_3

3-4-3 Efficiency of solar cells (P-n)

Figure (7) presents the (I-V) curves of the heterojunction fabricated by spray pyrolysis. Based on the (I-V) curve, the fill factor (FF) and photoelectric conversion efficiency (η) were calculated using formulae (5) and (6) respectively. according to the (I-V) curve. The heterojunction 9% Sb-doped Bi2O3 /n-psi showed the highest efficiency, with a value of (0.363 %). This is due to a reduction in structural defects, as a result, there is an increase in mobility .Thus, it contributes to the transfer of current and increases the spread states, thus increasing the photocurrent.

$$FF = \frac{I_{mp} \times V_{mp}}{I_{SC} \times V_{OC}} \quad \text{..... (5)}$$

Where: FF is Fill Factor, I_{mp} is the current at the maximum power point, V_{mp} is the voltage at the maximum power point, I_{SC} is Short Circuit Current, V_{OC} is Open-Circuit Voltage.

$$PCE = (\eta) = \frac{P_{out}}{P_{in}} \frac{J_{sc} V_{oc} FF}{P_{in}} \quad \text{....(6)}$$

Where: η is the efficiency of a solar cell, P_{out} is the power output, P_{in} is power input

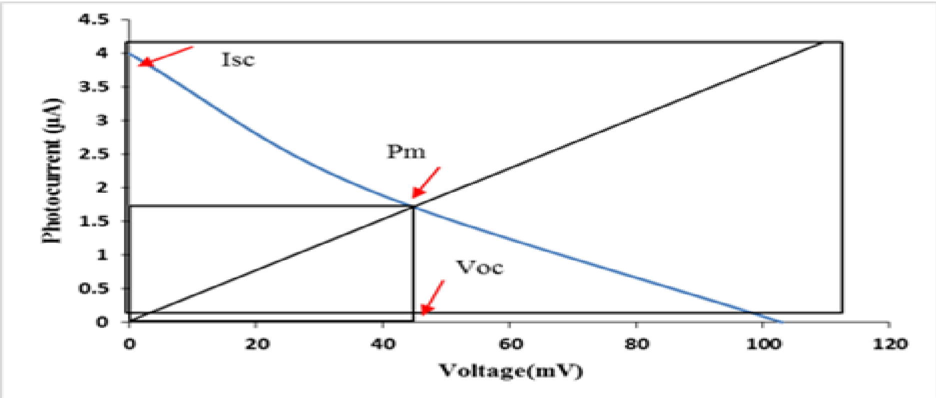

(a)

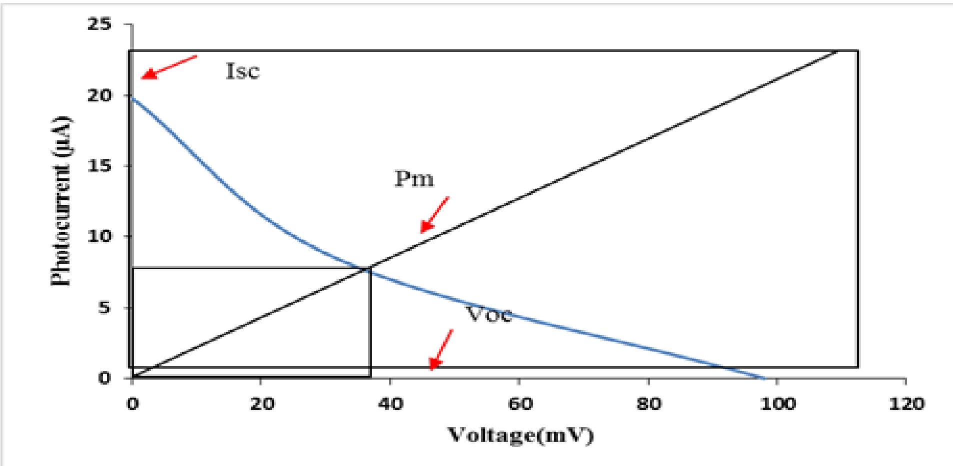

(b)

Figure (7) : Efficiency of solar cells for (a) undoped Bi_2O_3 (b) 9% Sb doped Bi_2O_3 and (c) 9% Al doped Bi_2O_3

Conclusions

1. X-ray diffraction tests reveal that spray-pyrolysed bismuth oxide (Bi_2O_3) thin films with and without doping have a polycrystalline structure and grow in the direction (002) that doping films prefer.
2. All thin films have a transmittance that rises as wavelength increases in the 350–900 nm regions.
3. When the concentration of Sb doping raises, the band gap decreases.
4. Undoped samples of 9% Sb-doped Bi2O3 display high-quality solar cell components. For 9%
5. Sb-doped Bi2O3, the efficiency of solar cells is 0.36.

References

[1] Sharma, P., & Katyal, S. C. (2010). Linear and nonlinear refractive index of As–Se–Ge and Bi doped As–Se–Ge thin films. Journal of Applied physics, 107(11).

[2] Hall, D. W., Newhouse, M. A., Borrelli, N. F., Dumbaugh, W. H., & Weidman, D. L. (1989). Nonlinear optical susceptibilities of high-index glasses. Applied Physics Letters, 54(14), 1293-1295.

[3] Stehle, C., Vira, C., Hogan, D., Feller, S., & Affatigato, M. (1998). Optical and physical properties of bismuth borate glasses related to structure. Physics and Chemistry of Glasses, 39(2), 83-86.

[4] Yiannopoulos, Y. D., Chryssikos, G. D., & Kamitsos, E. I. (2001). Structure and properties of alkaline earth borate glasses. Physics and chemistry of glasses, 42(3), 164-172.

[5] Pan, A., & Ghosh, A. (2000). A new family of lead–bismuthate glass with a large transmitting window. Journal of non-crystalline solids, 271(1-2), 157-161.

[6] Dolocan, V., & Iova, F. (1981). Optical properties of Bi2O3 thin films. physica status solidi (a), 64(2), 755-759.

[7] Leontie, L., Caraman, M., Delibaş, M., & Rusu, G. I. (2001). Optical properties of bismuth trioxide thin films. Materials Research Bulletin, 36(9), 1629-1637.

[8] Leontie, L., Caraman, M., & Rusu, G. I. (2000). On the photoconductivity of Bi2O3 in thin films. Journal of optoelectronics and Advanced Materials, 385-389.

[9] Shuk, P., Wiemhöfer, H. D., Guth, U.¨., Göpel, W., & Greenblatt, M. (1996). Oxide ion conducting solid electrolytes based on Bi2O3. Solid State Ionics, 89(3-4), 179-196.

[10] Gualtieri, A. F., Immovilli, S., & Prudenziati, M. (1997). Powder X-ray diffraction data for the new polymorphic compound ω-Bi2O3. Powder Diffraction, 12(2), 90-92.

[11] Moiseev, G., Vatolin, N., & Belousova, N. (2000). Thermodynamic investigations in the Bi-O system. Journal of thermal analysis and calorimetry, 61(1), 289-303.

[12] Risold, D., Hallstedt, B., Gauckler, L. J., Lukas, H. L., & Fries, S. G. (1995). The bismuth-oxygen system. Journal of phase equilibria, 16, 223-234.

[13] Zhukov, V. P., Zhukovskii, V. M., Zainullina, V. M., & Medvedeva, N. I. (1999). Electronic structure and chemical bonding in bismuth sesquioxide polymorphs. Journal of Structural Chemistry, 40, 831-837.

[14] Gobrecht, H., Seeck, S., Bergt, H. E., Märtens, A., & Kossmann, K. (1969). Investigations on evaporated films of bismuth oxide ii. determination of type of conductivity and photoconductivity measurements on doped and undoped layers. physica status solidi (b), 34(2), 569-576.

[15] George, J. (1987). 513; J. George, B. Pradeep, KS Joseph. Phys. Stat. Sol.(a), 108, 607.

[16] Yu, B., Zhu, C., & Gan, F. (1997). Optical nonlinearity of Bi2O3 nanoparticles studied by Z-scan technique. Journal of applied physics, 82(9), 4532-4537.

[17] Stark, W. J., Stoessel, P. R., Wohlleben, W., & Hafner, A. J. C. S. R. (2015). Industrial applications of nanoparticles. *Chemical Society Reviews*, *44*(16), 5793-5805.

[18] Kuz'Menko, A. B., Tishchenko, E. A., & Orlov, V. G. (1996). Transverse optic modes in monoclinic. Journal of Physics: Condensed Matter, 8(34), 6199.

[19] Pradeep, T. (2008). Nano: the essentials: understanding nanoscience and nanotechnolgy. (No Title).

[20] Darweesh, H. H. M. (2018). Nanomaterials: classification and properties-Part I. Journal of Nanoscience, 1(1), 1-11.

[21] Anderson, A. L., Chen, S., Romero, L., Top, I., & Binions, R. (2016). Thin films for advanced glazing applications. Buildings, 6(3), 37.

[22] Babar, A. R., Shinde, S. S., Moholkar, A. V., Bhosale, C. H., Kim, J. H., & Rajpure, K. Y. (2010). Structural and optoelectronic properties of antimony incorporated tin oxide thin films. Journal of Alloys and Compounds, 505(2), 416-422.

[23] M. M. Kareem, Z. T. Khodair, F. Y. Mohammed, (2020). Effect of annealing temperature on structural, morphological and optical properties of ZnO nanorod thin films prepared by hydrothermal method, Journal of Ovonic Research, Vol. 16, No. 1. January-februray 2020. P.53-61

[24] A. M. Saleh , N. A. Bakr, Z. T. Khodair,(2018). Effect of oxygen flow rate on structural and optical properties of SnO_2 thin films prepared by APCVD technique, Digest Journal of Nanomaterials and Biostructures Vol. 13, No. 3, July - September 2018, p. 603 – 608

[25] C.K.De, and N. K. Misra, “X-ray diffraction analysis o f lattice defects of ZnSe thin film s deposited at different substrate tem peratures,” Indian J. Phys.71A , pp. 535-544, 1997.

[26] Dimova-Malinovska, D., Marshall, J. M., & Vaseashta, A. (2005). Nanostructured and advanced materials for applications in sensor, optoelectronic and photovoltaic technology. Springer.

[27] Bensahel, B., Canham, L. T., & Ossicini, S. (Eds.). (2012). Optical properties of low dimensional silicon structures (Vol. 244). Springer Science & Business Media.

[28] Green, M. A. (1982). Solar cells: operating principles, technology, and system applications. Englewood Cliffs.

[29] Klug, H. P. (1974). X-ray diffraction procedures for polycrystalline and amorphous materials.